Tunnel magnetoresistance in fully epitaxial magnetic tunnel junctions with a full-Heusler alloy thin film of $Co_2Cr_{0.6}Fe_{0.4}Al$ and a MgO tunnel barrier

Takao Marukame and Masafumi Yamamoto[a)]
Division of Electronics for Informatics, Graduate School of Information Science and Technology, Hokkaido University, N14, W9, Kita-ku, Sapporo 060-0814, Japan

(Received 17 January 2007; accepted 13 February 2007; published online 30 April 2007)

Fully epitaxial magnetic tunnel junctions (MTJs) were fabricated with a full-Heusler alloy $Co_2Cr_{0.6}Fe_{0.4}Al$ (CCFA) thin film and a MgO tunnel barrier. Pseudo-spin-valve-type, fully epitaxial CCFA/MgO/$Co_{50}Fe_{50}$ MTJs with a CCFA film composition close to the stoichiometric one demonstrated high tunnel magnetoresistance (TMR) ratios of 90% at room temperature (RT) and 240% at 4.2 K. These high TMR ratios were attributed to the increased spin polarization at the Fermi level due to the increased ratio of the *B*2 region to the *A*2 region in CCFA films achieved by bringing the CCFA film composition close to the stoichiometric one. Fully epitaxial CCFA/MgO/$Co_{50}Fe_{50}$ MTJs with exchange biasing were also fabricated, where a $Co_{50}Fe_{50}$ upper electrode was used in a synthetic ferrimagnetic $Co_{50}Fe_{50}$/Ru/$Co_{90}Fe_{10}$ trilayer exchange-biased with an IrMn layer through the $Co_{90}Fe_{10}$/IrMn interface. These exchange-biased CCFA/MgO/$Co_{50}Fe_{50}$ MTJs exhibited further enhanced TMR ratios of 109% at RT and 317% at 4.2 K. We suggested enhancement of the TMR ratio by a coherent tunneling contribution for fully epitaxial CCFA/MgO/$Co_{50}Fe_{50}$ MTJs. © *2007 American Institute of Physics*.
[DOI: 10.1063/1.2718284]

I. INTRODUCTION

In the field of spintronics, where the spin of the electron is employed as an additional degree of freedom in electronics, it is essential to generate highly spin-polarized conduction electrons and transport them.[1] Half-metallic ferromagnets (HMFs) are characterized by an energy gap at the Fermi level (E_F) for one spin direction, leading to a complete spin polarization at E_F (Ref. 2). The potentially high spin polarization of HMFs is highly preferable for spintronic devices.

Co-based full-Heusler alloy thin films have been studied intensively[3–12] because of the half-metallic ferromagnetic nature theoretically predicted for some of these alloys[13,14] and because of their high Curie temperatures, which are well above room temperature (RT) (Ref. 15). The potentially high spin polarization of Co-based full-Heusler alloys is greatly advantageous for achieving high tunnel magnetoresistance (TMR) ratios in magnetic tunnel junctions (MTJs) (Refs. 16–33) and high magnetoresistance ratios in giant magnetoresistance devices.[34,35] It is also advantageous for efficient spin injection from ferromagnetic electrodes into semiconductors[36,37] and current-induced magnetization switching in MTJs.

One Co-based full-Heusler alloy, in particular, $Co_2Cr_{0.6}Fe_{0.4}Al$ (CCFA), features theoretically predicted high spin polarizations for both the ordered $L2_1$ structure and the disordered *B*2 one,[38] along with a relatively high T_c around 750 K.[39,40] The spin polarization theoretically predicted for the $L2_1$ structure is 0.90 and that for the *B*2 one is 0.78.[38] The structural and magnetic properties of bulk CCFA (Refs. 39–41) and epitaxially grown CCFA thin films[8–10,21,26] have been investigated.

Inomata *et al.* first demonstrated a relatively high TMR ratio of 16% at RT for MTJs using a Co-based full-Heusler alloy thin film, where a polycrystalline CCFA thin film as a lower electrode and an amorphous AlO_x tunnel barrier were used.[16] Subsequently, relatively high TMR ratios of up to 70% at RT have been shown for MTJs using a Co-based full-Heusler alloy thin film—Co_2MnSi (Ref. 19), Co_2FeAl (Refs. 20 and 25), or Co_2MnAl (Ref. 23)—and an amorphous AlO_x tunnel barrier. Sakuraba *et al.* reported a high TMR ratio of 570% at 2 K (67% at RT) for MTJs consisting of an epitaxially grown Co_2MnSi lower electrode, an amorphous AlO_x tunnel barrier, and a highly oriented Co_2MnSi upper electrode.[24]

We fabricated single-crystal, epitaxially grown Co_2YZ thin films of CCFA (Refs. 21 and 26), Co_2MnGe (Ref. 11), or Co_2MnSi (Ref. 12) on MgO-buffered MgO(001) substrates. Given these epitaxial thin films, we developed fully epitaxial MTJs that had a Co_2YZ thin film of CCFA,[21,26] Co_2MnGe,[26,27] or Co_2MnSi (Refs. 30–32) as a lower electrode, a MgO tunnel barrier, and a $Co_{50}Fe_{50}$ upper electrode. We reported fully epitaxial CCFA/MgO/$Co_{50}Fe_{50}$ MTJs showing relatively high TMR ratios of 42% at RT and 74% at 55 K.[21,26] However, the CCFA thin film composition used in this previous study was $Co_2(Cr_{0.61}Fe_{0.38})Al_{0.81}$ and significantly deviated from the stoichiometric one of 2:1:1 (Ref. 26). Hereafter, we refer to the CCFA film with this composition as CCFA film A. We represent the fabricated Co_2YZ film composition as $Co_2Y_aZ_b$, where Y_a stands for $Cr_{a1}Fe_{a2}$ ($a=a1+a2$) and Z_b stands for Al_b for CCFA; that is, *a*

[a)]Author to whom correspondence should be addressed; electronic mail: yamamoto@nano.ist.hokudai.ac.jp

=0.99, b=0.81, and $a+b$=1.80 for CCFA film A. Deviation of the film composition from the stoichiometric one inevitably results in structural defects, which may reduce the spin polarization of E_F (Refs. 38 and 42). Furthermore, in our previous CCFA/MgO/$Co_{50}Fe_{50}$ MTJs, the parallel and antiparallel magnetization configurations were controlled by using the difference in the coercive forces between the CCFA lower electrode and the $Co_{50}Fe_{50}$ upper electrode (i.e., they were pseudo-spin-valve-type MTJs). This resulted in peaked magnetoresistance versus magnetic field characteristics,[21] which probably led to TMR ratios lower than they potentially could be. Exchange biasing is favorable for realizing high degrees of the parallel and antiparallel magnetization configurations.[43]

Our purpose in this study was to improve the TMR characteristics of fully epitaxial MTJs with a full-Heusler alloy thin film of CCFA as a lower electrode, a MgO tunnel barrier, and a $Co_{50}Fe_{50}$ upper electrode, and demonstrate a potentially high tunneling spin polarization of CCFA. To do this, we took two approaches. The first was to fabricate pseudo-spin-valve-type, fully epitaxial CCFA/MgO/$Co_{50}Fe_{50}$ MTJs with a CCFA film composition close to the stoichiometric one of 2:1:1. The second was to develop fully epitaxial CCFA/MgO/$Co_{50}Fe_{50}$ MTJs with exchange biasing.

In Sec. II, we describe our experimental methods. The preparation of MTJ layer structures in an ultrahigh vacuum chamber through the combined use of magnetron sputtering and electron evaporation is described. In Sec. III, we present experimental results regarding structural characterization of fabricated CCFA thin films and CCFA/MgO/$Co_{50}Fe_{50}$ MTJ layer structures. In Sec. III, we also describe the experimentally obtained TMR characteristics of the fully epitaxial CCFA/MgO/$Co_{50}Fe_{50}$ MTJs. The pseudo-spin-valve-type, fully epitaxial MTJs with a CCFA film composition close to the stoichiometric one showed a TMR ratio of 90% at RT (240% at 4.2 K).[28] We discuss a possible reason for the increased TMR ratio, compared with a previously obtained value of 42% at RT (74% at 55 K) for CCFA/MgO/$Co_{50}Fe_{50}$ MTJs with a CCFA film composition which significantly deviated from the stoichiometric one, in terms of the increased $B2$ ratio achieved by bringing the CCFA film composition closer to the stoichiometric one. Furthermore, we have demonstrated a high TMR ratio of 109% at RT (317% at 4.2 K) for fully epitaxial CCFA/MgO/$Co_{50}Fe_{50}$ with exchange biasing.[33] We have estimated a tunneling spin polarization of 0.88 at 4.2 K for epitaxial CCFA films with the $B2$ structure from the experimentally obtained TMR ratios and suggested enhancement of the TMR ratio by a coherent tunneling contribution for fully epitaxial CCFA/MgO/$Co_{50}Fe_{50}$ MTJs. In Sec. IV, we summarize our results and conclude.

II. EXPERIMENTAL METHODS

Full-Heusler alloys are ternary intermetallic compounds with the composition X_2YZ in the $L2_1$ cubic structure (space group: $Fm\bar{3}m$). A typical full-Heusler alloy consists of two different transition metals X and Y and a nonmagnetic element Z, as shown in Fig. 1(a). The lattice consists of four

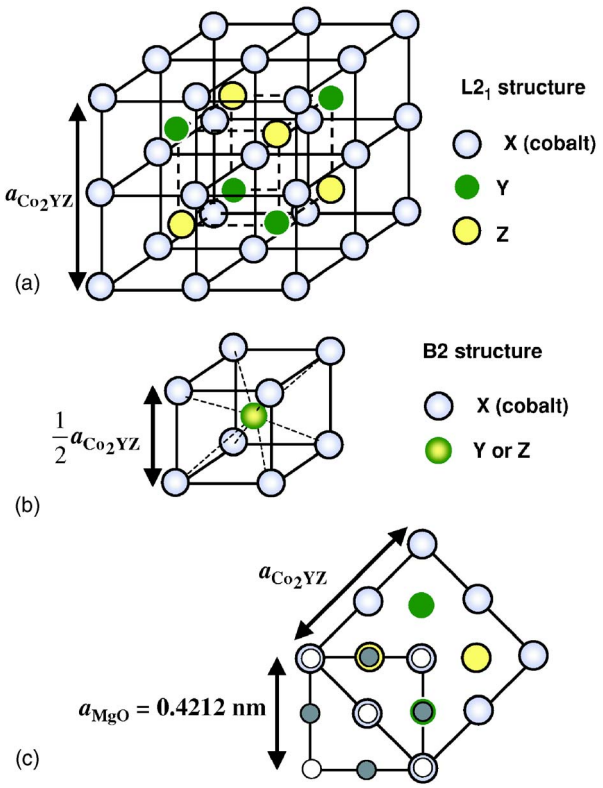

FIG. 1. (Color online) (a) Schematic view of the $L2_1$ crystal structure with composition X_2YZ. The lattice consists of four different fcc sublattices. Each has an atom basis as follows: X element at (0, 0, 0) and (1/2,1/2,1/2), Y at (1/4,1/4,1/4), and Z at (3/4,3/4,3/4). (b) Schematic view of the $B2$ crystal structure with composition X_2YZ. (c) Top view of Heusler alloy crystal structure ($L2_1$ structure). MgO cubic structure is superimposed.

different fcc sublattices. Each has an atom basis as follows: X element at (0, 0, 0) and (1/2, 1/2, 1/2), Y at (1/4, 1/4, 1/4), and Z at (3/4, 3/4, 3/4). The Y-Z-type disordered X_2YZ has the $B2$ structure [Fig. 1(b)]. The lattice mismatch between CCFA [lattice constant a=0.5737 nm (Refs. 39 and 40)] and MgO (a=0.4212 nm) on a 45° in-plane rotation is relatively small, about −3.7%. Therefore, it is reasonable to expect that CCFA films will grow epitaxially with their [100] direction rotated by 45° from the MgO [100] direction in the (001) plane [Fig. 1(c)]. Similarly, the lattice mismatch between $Co_{50}Fe_{50}$ [lattice constant a=0.2850 nm (Ref. 44)] and MgO on a 45° in-plane rotation is relatively small, about −4.3%. We can also expect that $Co_{50}Fe_{50}$ films will grow epitaxially on MgO with the $Co_{50}Fe_{50}$ [100] direction rotated by 45° from the MgO [100] direction in the (001) plane.

We fabricated two sets of MTJ layer structures. The first set was pseudo-spin-valve-type, fully epitaxial CCFA/MgO/$Co_{50}Fe_{50}$ MTJs with a CCFA film composition close to the stoichiometric one. For this type of MTJ, we used a wedge-shaped MgO tunnel barrier so that we could investigate the TMR characteristics as a function of MgO barrier thickness. The nominal thickness of the MgO tunnel barrier (t_{MgO}) was varied from 1.0 to 3.6 nm on each 20 × 20 mm substrate by using a linearly moving shutter during the deposition. The fabricated epitaxial MTJ layer structure (from the substrate side) was MgO buffer layer (10 nm)/CCFA lower electrode (50 nm)/MgO tunnel bar-

rier (1.0–3.6 nm)/$Co_{50}Fe_{50}$ upper electrode (30 nm), grown on a MgO(001) single-crystal substrate. The $Co_{50}Fe_{50}$ layer, which had a coercive force higher than that of the CCFA layer, was deposited at RT using magnetron sputtering. The composition of the CCFA film used in the first set of MTJs was $Co_{2.0}Cr_{0.56}Fe_{0.40}Al_{0.99}$ as determined through inductively coupled plasma (ICP) analysis with an accuracy of 2%–3% for the composition of each element. We refer to the CCFA film with this composition as CCFA film B (a=0.96, b=0.99, $a+b$=1.95). Thus, the film composition was brought close to the stoichiometric one of 2:1:1 for $Co_2(Cr_{0.6}Fe_{0.4})Al$, in contrast with that of the $Co_2Cr_{0.61}Fe_{0.38}Al_{0.81}$ (CCFA film A, $a+b$=1.80) used to fabricate the CCFA MTJs which showed TMR ratios of about 42% at RT.[21,26]

The second set was fully epitaxial CCFA/MgO/$Co_{50}Fe_{50}$ MTJs with exchange biasing. We used an upper electrode of $Co_{50}Fe_{50}$ film in an antiferromagnetically coupled (i.e., synthetic ferrimagnetic) $Co_{50}Fe_{50}$/Ru/$Co_{90}Fe_{10}$ trilayer exchange-biased by an IrMn antiferromagnetic layer through the $Co_{90}Fe_{10}$/IrMn interface to obtain a high value of exchange-bias field (H_{ex}) for epitaxial $Co_{50}Fe_{50}$ electrodes.[45] We confirmed that the $Co_{50}Fe_{50}$/Ru/$Co_{90}Fe_{10}$ trilayers, which had a typical Ru interlayer thickness of 0.8 nm, behaved magnetically as synthetic ferrimagnets. The fabricated MTJ layer structure in this case was as follows: (from the substrate side) MgO buffer layer (10 nm)/CCFA (50 nm)/MgO barrier (2.4 nm)/$Co_{50}Fe_{50}$ (3.4 nm)/Ru (0.8 nm)/$Co_{90}Fe_{10}$ (2 nm)/IrMn (10 nm)/Ru cap (5 nm). The 5-nm-thick Ru cap layer was used to protect the IrMn layer from corrosion. The composition of the CCFA film used in the second set of MTJs was determined through ICP analysis to be $Co_2Cr_{0.57}Fe_{0.39}Al_{1.12}$. We refer to the CCFA film with this composition as CCFA film C (a=0.96, b=1.12, $a+b$=2.08).

All layers in these MTJs were successively deposited on MgO(001) single-crystal substrates in an ultrahigh vacuum chamber (with a base pressure of about 8×10^{-8} Pa) through the combined use of magnetron sputtering and electron beam evaporation. The CCFA lower electrode was deposited by rf magnetron sputtering at RT and subsequently annealed *in situ* at 500 °C for 15 min. The MgO tunnel barrier was deposited by electron beam evaporation at RT. The pressure during the deposition of the MgO tunnel barrier was about 6×10^{-7} Pa. The layers of $Co_{50}Fe_{50}$, Ru, $Co_{90}Fe_{10}$, and IrMn were all deposited by magnetron sputtering at RT.

The structural characterization for the fabricated CCFA thin films and CCFA MTJs were performed using *in situ* reflection high-energy electron diffraction (RHEED), x-ray Bragg scans, x-ray pole figure measurements (Bruker AXS D8 DISCOVER Hybrid), cross-sectional high-resolution transmission electron microscope (HRTEM) observation, and transmission electron diffraction.

We fabricated MTJs with the fully epitaxial layer structures described above by photolithography and Ar ion milling. The fabricated junction sizes were 8×8 μm^2 for the first set of MTJs and 10×10 μm^2 for the second set. After the microfabrication procedure, some of the MTJs were annealed at 175 °C for 1 h in a vacuum of 10^{-4} Pa under a magnetic field of 5 kOe. The magnetoresistance was measured with a magnetic field applied along the [110] axis of the CCFA at temperatures from 4.2 K to RT using a dc four-probe method. We defined the TMR ratio as $(RA_{AP}-RA_P)/RA_P$, where RA_{AP} and RA_P are the respective resistance-area products for the antiparallel and parallel magnetization configurations between the upper and lower electrodes.

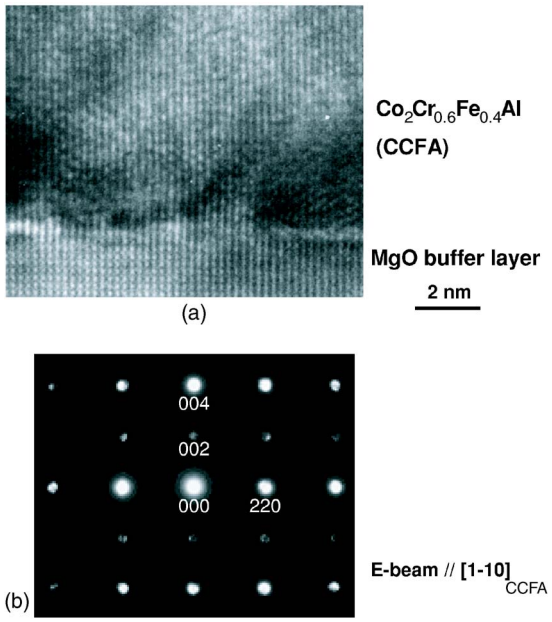

FIG. 2. (Color online) (a) Cross-sectional high-resolution transmission electron microscope image of $Co_2Cr_{0.6}Fe_{0.4}Al$ (CCFA) (50 nm)/MgO buffer layer, along the [1-10] direction of the CCFA. (b) Electron diffraction pattern for the CCFA layer. The electron-beam diameter was 10 nm.

III. EXPERIMENTAL RESULTS AND DISCUSSION

A. Structural properties of CCFA thin films and CCFA/MgO/$Co_{50}Fe_{50}$ MTJ layer structures

We will first describe the structural properties of the fabricated CCFA thin films. We used x-ray pole figure measurements to confirm that the fabricated 50-nm-thick CCFA thin films with CCFA films B and C annealed *in situ* at 500 °C were grown epitaxially on MgO-buffered MgO(001) substrates and crystallized in the $B2$ structure. The crystallographic relationship was CCFA (001) [100]∥MgO (001) [011]. These results were in agreement with our previous work.[21,26] Figure 2(a) shows a cross-sectional high-resolution TEM lattice image, along the [1-10] direction of the CCFA film, of a 500 °C annealed CCFA (50 nm) thin film (CCFA film B) deposited on a MgO buffer layer. As can be seen in Fig. 2(a), the TEM lattice image clearly showed that the CCFA film was grown epitaxially on a MgO-buffered MgO(001) substrate and was single crystalline. Figure 2(b) shows a microbeam electron diffraction pattern with a beam diameter of 10 nm for the CCFA film. In the electron diffraction pattern, 002 spots were observed, while 111 spots were not observed. These results—i.e., the existence of 002 spots and the lack of 111 spots—indicated that the 500 °C annealed CCFA films with the film composition of $Co_{2.0}Cr_{0.56}Fe_{0.40}Al_{0.99}$ grown on MgO buffer layers had the

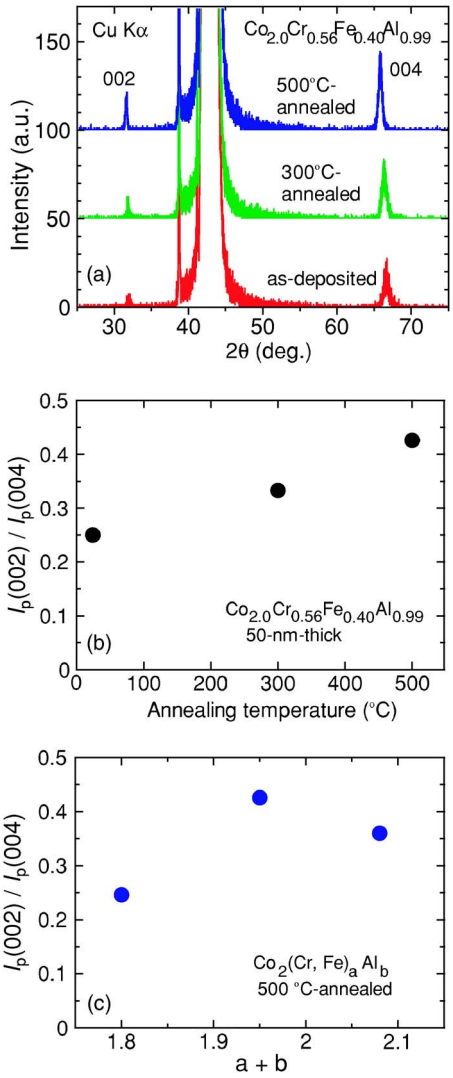

FIG. 3. (Color online) (a) X-ray θ-2θ diffraction patterns of 50-nm-thick as-deposited, 300 °C annealed, and 500 °C annealed CCFA films deposited on MgO-buffered MgO(001) substrates. The film composition was $Co_{2.0}Cr_{0.56}Fe_{0.40}Al_{0.99}$. (b) Peak intensity ratio of $I_P(002)/I_P(004)$ for the CCFA thin films [these are the same films shown in (a)] as a function of *in situ* postdeposition annealing temperature. (c) Peak intensity ratio of $I_P(002)/I_P(004)$ for the CCFA thin films annealed *in situ* at 500 °C as a function of the film composition $a+b$ in the representation composition of $Co_2(Cr,Fe)_aAl_b$.

*B*2 structure, and so were consistent with the results obtained through x-ray pole figure measurements.

Figure 3(a) shows x-ray θ-2θ diffraction patterns of 50-nm-thick as-deposited, 300 °C and 500 °C annealed CCFA films [film composition: $Co_{2.0}Cr_{0.56}Fe_{0.40}Al_{0.99}$ (CCFA film B)]; clear 002 and 004 peaks were observed even for the as-deposited films. As shown in Fig. 3(a), annealing the as-deposited CCFA film at temperatures ranging from 300 to 500 °C caused the intensities (I_P) of 002 and 004 peaks to increase. This result was similar to that for the $Co_2Cr_{0.61}Fe_{0.38}Al_{0.81}$ (CCFA film A) used to fabricate CCFA MTJs which showed TMR ratios of about 42% at RT.[21,26] Furthermore, the peak intensity ratio of $I_P(002)/I_P(004)$ rose with increasing annealing temperature [Fig. 3(b)]. This suggests that the ratio of the *B*2 structure region to the *A*2 structure region was increased by *in situ* postdeposition annealing.

We next investigated the relative intensities of x-ray diffraction 002 and 004 peaks for CCFA films as a function of the film composition. Note that the 002 peak is specific to the *B*2 structure. If we use a parameter q to represent the ratio of the 002 peak intensity, $I_P(002)$, to the 004 peak intensity, $I_P(004)$, q corresponds to the ratio of the *B*2 region to the *A*2 region (the *B*2 ratio).

$$q = \frac{I_P(002)}{I_P(004)}. \tag{1}$$

Figure 3(c) shows the peak intensity ratio of $I_P(002)/I_P(004)$ for the CCFA films (50 nm) deposited at RT on MgO buffer layers (10 nm) and subsequently annealed *in situ* at 500 °C as a function of the film composition of $a+b$. Compared to the peak intensity ratio of $I_P(002)/I_P(004)$ for our previous CCFA thin film with a film composition which deviated significantly from the stoichiometric one of 2:1:1 (CCFA film A: $Co_2Cr_{0.61}Fe_{0.38}Al_{0.81}$, $a+b=1.80$), that of the CCFA thin film with a composition close to the stoichiometric one (CCFA film B, $Co_{2.0}Cr_{0.56}Fe_{0.40}Al_{0.99}$, $a+b=1.95$) was markedly high. As shown in Fig. 3(c), the parameter q corresponding to the *B*2 ratio increased as the film composition approached the stoichiometric one of 2:1:1.

We will now describe the structural properties of the fabricated MTJ structures. First, we describe the structural properties of the fabricated pseudo-spin-valve-type, fully epitaxial CCFA/MgO/$Co_{50}Fe_{50}$ MTJs with a CCFA film composition close to the stoichiometric one (CCFA film B). RHEED patterns observed *in situ* for each layer during fabrication clearly indicated that the CCFA lower electrode, MgO tunnel barrier, and $Co_{50}Fe_{50}$ upper electrode grew epitaxially. We also performed a cross-sectional high-resolution TEM observation for a CCFA (50 nm)/MgO (2 nm)/$Co_{50}Fe_{50}$ (30 nm) MTJ layer structure along the [110] direction of the CCFA film. The observed TEM lattice image clearly showed that all the layers of the CCFA/MgO/$Co_{50}Fe_{50}$ MTJ structure were grown epitaxially and were single crystalline. It also confirmed that extremely smooth and abrupt interfaces were formed.[28]

Second, we will describe the structural properties of the fully epitaxial CCFA/MgO/$Co_{50}Fe_{50}$ MTJs with exchange biasing. In the MTJ structure, CCFA films with the composition of $Co_2Cr_{0.57}Fe_{0.39}Al_{1.12}$ (CCFA film C) were used. The basic tunnel junction trilayers of the CCFA/MgO/$Co_{50}Fe_{50}$ MTJs with exchange biasing were the same as those of the pseudo-spin-valve-type MTJs described above, except that the thickness of the $Co_{50}Fe_{50}$ upper electrode (t_{CoFe}) was decreased to 3.4 nm from t_{CoFe} of 30 nm. RHEED patterns observed *in situ* for each layer during fabrication clearly indicated that the CCFA lower electrode, MgO tunnel barrier, and $Co_{50}Fe_{50}$ upper electrode grew epitaxially. Figure 4 shows a cross-sectional high-resolution TEM lattice image of the fabricated MTJ layer structure from the CCFA layer to the IrMn layer. This cross-sectional HRTEM image clearly shows that all the layers of the CCFA/MgO/$Co_{50}Fe_{50}$ basic tunnel junction trilayer were grown epitaxially and were single crystalline. It also confirmed that extremely smooth and abrupt interfaces were formed.

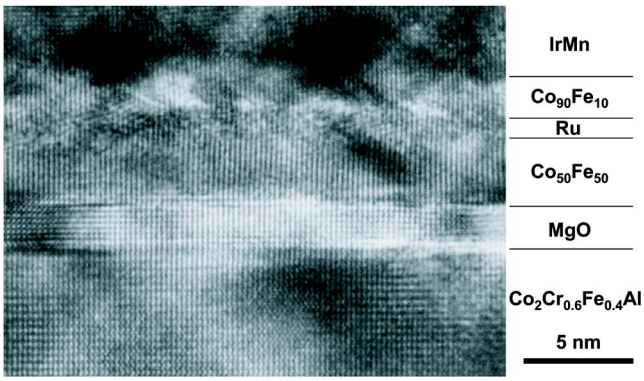

FIG. 4. (Color online) Cross-sectional high-resolution transmission electron microscope image of a MTJ layer structure, consisting of $Co_2Cr_{0.6}Fe_{0.4}Al$ (CCFA) (50 nm)/MgO (2 nm)/$Co_{50}Fe_{50}$ (3 nm)/Ru (0.8 nm)/$Co_{90}Fe_{10}$ (2 nm)/IrMn (10 nm)/Ru cap (5 nm), along the [1–10] direction of the CCFA.

Next, we will describe the structural properties of the $Co_{50}Fe_{50}$/Ru/$Co_{90}Fe_{10}$/IrMn quadrilayers. We also observed streak patterns in the RHEED patterns, dependent on the incident directions of the electron beam, for layers of Ru, $Co_{90}Fe_{10}$, and IrMn, indicating that the layers grew epitaxially on the epitaxial $Co_{50}Fe_{50}$ electrode. Furthermore, cross-sectional HRTEM lattice images (Fig. 4) clearly showed that all the layers of Ru, $Co_{90}Fe_{10}$, and IrMn were also grown epitaxially on the single-crystal $Co_{50}Fe_{50}$ electrode and were single crystalline, although the detailed structures of the successive layers from the Ru interlayer to the IrMn layer were not fully analyzed.

B. TMR characteristics of pseudo-spin-valve-type CCFA/MgO/$Co_{50}Fe_{50}$ MTJs with a CCFA film composition close to the stoichiometric one

We will describe the TMR characteristics of the fabricated pseudo-spin-valve-type, fully epitaxial CCFA/MgO/$Co_{50}Fe_{50}$ MTJs with a CCFA film composition of $Co_{2.0}Cr_{0.56}Fe_{0.40}Al_{0.99}$ (CCFA thin film B), which was close to the stoichiometric one. The as-fabricated (i.e., not *ex situ* annealed) MTJs exhibited typical TMR ratios of 80% at RT and 210% at 4.2 K. Figure 5 shows RA_P and TMR ratios of the as-fabricated MTJs at RT as a function of t_{MgO}. A clear exponential dependence of RA_P on t_{MgO} was observed for a t_{MgO} range from 1.1 to 2.5 nm, indicating typical tunnel junction behavior. The $m^*\varphi_0$ value estimated from the slope of $\ln(RA_P)$ vs t_{MgO} according to the Wenzel-Kramer-Brillouin (WKB) approximation was 0.32 eV for the CCFA MTJ, where m^* is the effective electron mass normalized by the bare electron mass and φ_0 is the potential barrier height (the energy difference between the Fermi level of the emitter ferromagnetic electrode and the bottom of the conduction band in the tunnel barrier).[46] This value was close to that of 0.39 eV obtained for epitaxial Fe/MgO/Fe MTJs.[47] Relatively high TMR ratios from 60% to 83% were obtained at RT for a wide range of t_{MgO} from 1.1 to 2.5 nm.

The as-fabricated (i.e., not *ex situ* annealed) MTJs exhibited typical TMR ratios of 80% at RT and 210% at 4.2 K. Figure 6 shows typical magnetoresistance curves at V =5 mV at RT and 4.2 K for a MTJ postfabrication annealed

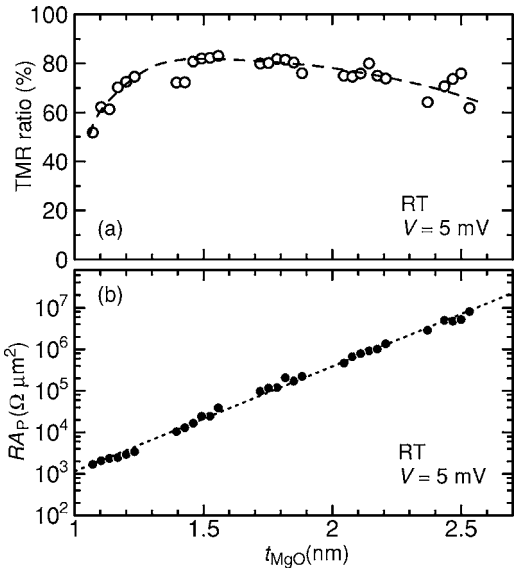

FIG. 5. MgO tunnel barrier thickness (t_{MgO}) dependence of (a) TMR ratio and (b) RA_P at RT (measured at a bias voltage of 5 mV) for as-fabricated (i.e., not *ex situ* annealed) $Co_2Cr_{0.6}Fe_{0.4}Al$/MgO/$Co_{50}Fe_{50}$ MTJs. RA_P represents the resistance-area product for the parallel magnetization configuration. The scale of the vertical axis for RA_P is logarithmic. The dashed line serves as a guide to the eye. The dotted line represents a least-squares approximation of the form $\ln(RA_P)=A+B\cdot t_{MgO}$.

at 175 °C. The MgO tunnel barrier thickness was 1.6 nm. The annealed MTJs showed increased TMR ratios of 90% at RT and 240% at 4.2 K. The significant increase of the TMR ratio in the epitaxial CCFA MTJs compared to our previously reported value of about 42% at RT (Refs. 21 and 26) indicates that a film composition close to the stoichiometric one is essential to obtain high spin polarizations in CCFA thin films.

Now we will discuss a possible reason for the improved TMR ratios of the MTJs with a CCFA film having a composition close to the stoichiometric one. As described in Sec. III A, our x-ray diffraction (XRD) analysis for the epitaxially

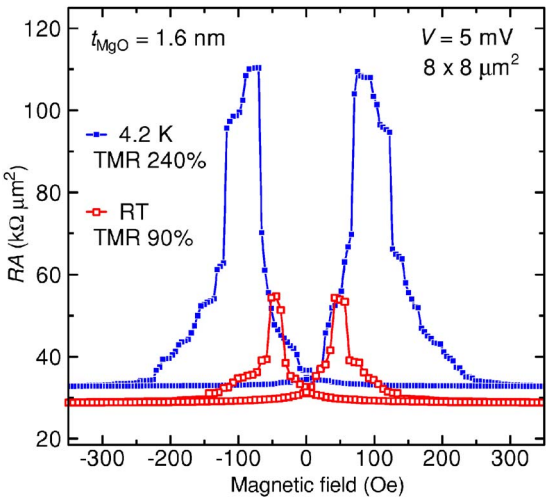

FIG. 6. (Color online) Typical magnetoresistance curves for a pseudo-spin-valve-type, epitaxial $Co_2Cr_{0.6}Fe_{0.4}Al$/MgO/$Co_{50}Fe_{50}$ MTJ *ex situ* annealed at 175 °C (t_{MgO}=1.6 nm) at a bias voltage of 5 mV at 4.2 K and RT. The junction size was 8×8 μm^2. The TMR ratios were 90% (RT) and 240% (4.2 K).

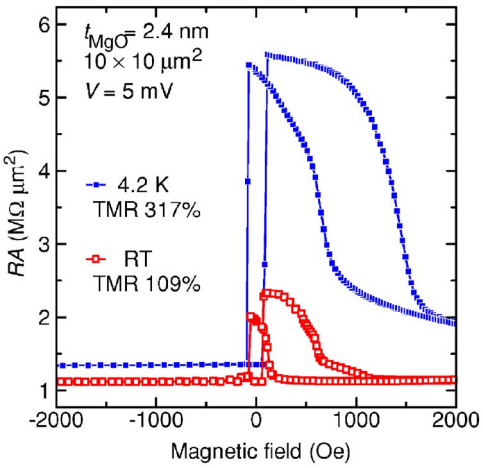

FIG. 7. (Color online) Typical magnetoresistance curves at RT and 4.2 K for a fully epitaxial $Co_2Cr_{0.6}Fe_{0.4}Al/MgO$ (2.4 nm)/$Co_{50}Fe_{50}$ MTJ with exchange biasing.

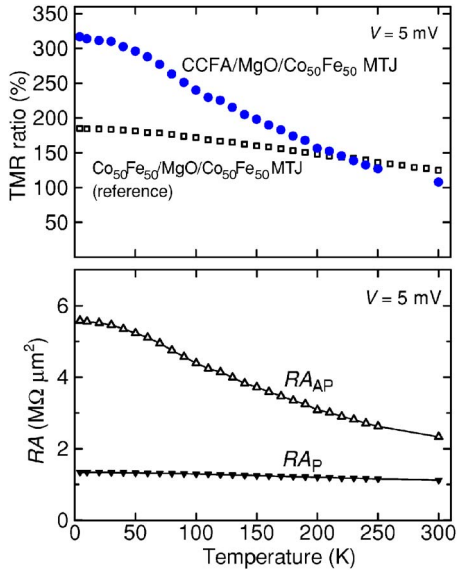

FIG. 8. (Color online) TMR ratios and RA_{AP} and RA_P for a fully epitaxial, exchange-biased $Co_2Cr_{0.6}Fe_{0.4}Al/MgO/Co_{50}Fe_{50}$ MTJ as a function of temperature from 4.2 K to RT, where RA_{AP} and RA_P represent the respective junction resistance-area products for the antiparallel and parallel magnetization configurations.

grown CCFA films indicated that the ratio of the $B2$ structure region to the $A2$ structure region (the $B2$ ratio) was increased by bringing the CCFA film composition close to the stoichiometric one of $a+b=2.0$. Theoretically, it was predicted that $A2$-type disorder would significantly decrease the spin polarization in Co_2CrAl while $B2$-type disorder would have little effect.[38] Therefore, we can reasonably attribute the observed TMR improvement to the increased spin polarization at E_F due to the increased $B2$ ratio.

C. TMR characteristics of CCFA/MgO/Co$_{50}$Fe$_{50}$ MTJs with exchange biasing

We will now describe the TMR characteristics of the fabricated fully epitaxial CCFA/MgO/$Co_{50}Fe_{50}$ MTJs with exchange biasing. In the MTJ structure, CCFA films with the composition of $Co_2Cr_{0.57}Fe_{0.39}Al_{1.12}$ (CCFA film C, $a+b=2.08$) were used.

Figure 7 shows typical magnetoresistance curves at RT and 4.2 K of a fabricated fully epitaxial, exchange-biased CCFA/MgO/$Co_{50}Fe_{50}$ MTJ. The applied bias voltage was 5 mV. The MTJ exhibited clear exchange-biased TMR characteristics with high TMR ratios of 109% at RT and 317% at 4.2 K. These values are significantly higher than the values of 90% at RT and 240% at 4.2 K for the pseudo-spin-valve-type, fully epitaxial CCFA/MgO/$Co_{50}Fe_{50}$ MTJs described in Sec. III B. We obtained relatively high H_{ex} values of about 350 Oe at RT and about 1000 Oe at 4.2 K, as shown in Fig. 7. We can reasonably attribute the high H_{ex} values obtained for the fabricated MTJs to a lower net saturation magnetization of the synthetic ferrimagnetic trilayer compared with a saturation magnetization of the $Co_{50}Fe_{50}$ electrode.

Figure 8 shows the TMR ratio for a fabricated fully epitaxial CCFA/MgO/$Co_{50}Fe_{50}$ MTJ (CCFA MTJ) with exchange biasing as a function of temperature (T) from 4.2 K to RT (the same MTJ shown in Fig. 7). For comparison, the TMR ratio as a function of T is also plotted for a fully epitaxial $Co_{50}Fe_{50}$/MgO/$Co_{50}Fe_{50}$ MTJ with exchange biasing (reference $Co_{50}Fe_{50}$ MTJ) identically fabricated with the same layer structure as that of the exchange-biased CCFA MTJ except that the lower electrode CCFA was replaced with $Co_{50}Fe_{50}$. The $Co_{50}Fe_{50}$ MTJs were postfabrication annealed under the same annealing conditions as for the CCFA MTJs (i.e., at 175 °C under a magnetic field of 5 kOe). The layer structure (from the substrate side) was MgO buffer layer (10 nm)/$Co_{50}Fe_{50}$ (50 nm)/MgO (2.2 nm)/$Co_{50}Fe_{50}$ (3 nm)/Ru (0.8 nm)/$Co_{90}Fe_{10}$ (2 nm)/IrMn (10 nm)/Ru (5 nm), grown on a MgO(001) single-crystal substrate. The $Co_{50}Fe_{50}$ MTJs showed TMR ratios of 185% at 4.2 K and 125% at RT. As shown in Fig. 8, the TMR ratio of the CCFA MTJ was higher than that of the $Co_{50}Fe_{50}$ MTJ below about 220 K, although it was slightly lower at RT. The comparison of the T dependences of the TMR ratios of the CCFA MTJ and $Co_{50}Fe_{50}$ MTJ definitely indicated that the higher TMR ratio for the CCFA MTJ below about 200 K, which reached 317% at 4.2 K, was due to a high tunneling spin polarization of the epitaxial CCFA electrode.

We next estimated the tunneling spin polarization of the epitaxial CCFA electrode from the obtained TMR ratios. The TMR ratios for MTJs have been traditionally related to the spin polarizations at E_F, P_1, and P_2, of the ferromagnetic electrodes through Jullière's model;[48] i.e.,

$$\mathrm{TMR} = 2P_1P_2/(1 - P_1P_2). \tag{2}$$

Jullière's model was derived by assuming a loss of coherence in tunneling (i.e., nonconservation of the electron's wave vector component parallel to the interface).[49] However, a straightforward application of Jullière's model for a TMR ratio of 317% at 4.2 K for the fully epitaxial CCFA/MgO/$Co_{50}Fe_{50}$ MTJ with a $Co_{50}Fe_{50}$ electrode spin polarization of 0.50, derived from dI/dV curves of superconductor/AlO_x/$Co_{50}Fe_{50}$ tunnel structures,[50] corresponding to the originally defined spin polarization using majority- and minority-spin band density of states at E_F, results in an unrealistically high P value exceeding 1.0 for the

epitaxial CCFA electrode. This result indicates enhancement of the TMR ratio by a coherent tunneling contribution[51,52] for fully epitaxial CCFA/MgO/$Co_{50}Fe_{50}$ MTJs. Furthermore, the obtained TMR ratios of 185% at 4.2 K and 125% at RT clearly indicate enhancement of the TMR ratio by a coherent tunneling contribution for the reference $Co_{50}Fe_{50}$ MTJs. Therefore, we estimated the tunneling spin polarization, or effective spin polarization for the epitaxial $Co_{50}Fe_{50}$ electrodes, P_{CoFe}, by applying Jullière's model for the TMR ratio of 185% at 4.2 K (125% at RT) of the reference $Co_{50}Fe_{50}$ MTJ. We obtained a P_{CoFe} value of 0.69 at 4.2 K (0.62 at RT), which was higher than the above P value of 0.50 derived from superconductor/AlO_x/$Co_{50}Fe_{50}$ tunnel structures.[50] Similarly, we estimated the tunneling spin polarization, or effective spin polarization for an epitaxial CCFA electrode in fully epitaxial CCFA/MgO/$Co_{50}Fe_{50}$ MTJs, P_{CCFA}, by applying Jullière's model for the TMR ratio of 317% at 4.2 K (109% at RT) of the CCFA MTJ, along with a P_{CoFe} value of 0.69 at 4.2 K (0.62 at RT) derived from the TMR ratio for the reference $Co_{50}Fe_{50}$ MTJ; in this case, we obtained a high tunneling spin polarization of 0.88 at 4.2 K (0.57 at RT) for the epitaxial CCFA thin film with the $B2$ structure. Although a rigorous comparison is not justified, the thus obtained P_{CCFA} value of 0.88 is larger than the theoretically predicted P_{CCFA} value of 0.78 (Ref. 38) even though we assumed an effective spin polarization of 0.69 at 4.2 K (0.62 at RT) for the epitaxial $Co_{50}Fe_{50}$ electrode in the estimation rather than 0.50 at 4.2 K which was derived from superconductor/AlO_x/$Co_{50}Fe_{50}$ tunnel structures. This result also indicates a coherent tunneling contribution[51,52] for fully epitaxial CCFA/MgO/$Co_{50}Fe_{50}$ MTJs.

Last, we will discuss the T dependence of the TMR ratio of the fully epitaxial CCFA/MgO/$Co_{50}Fe_{50}$ MTJs with exchange biasing. If we use parameter $\gamma = \alpha(4.2\ \mathrm{K})/\alpha(\mathrm{RT})$, where α is the TMR ratio, to represent the degree of the TMR ratio's T dependence, γ for the CCFA MTJs was 2.9. This γ value was higher than the value of 2.1 previously reported for CMS/MgO/$Co_{50}Fe_{50}$ MTJs [$\alpha(\mathrm{RT}) = 90\%$ and $\alpha(4.2\ \mathrm{K}) = 192\%$] (Refs. 30 and 31) and in contrast to a more moderate value of $\gamma = 1.5$ [$\alpha(\mathrm{RT}) = 125\%$ and $\alpha(4.2\ \mathrm{K}) = 185\%$] for the reference $Co_{50}Fe_{50}$ MTJs. Regarding the T dependences of RA_{AP} and RA_P, RA_{AP} decreased with increasing T, while RA_P was almost independent of T for the CCFA MTJs [Fig. 8(b)]. These T dependences of RA_{AP} and RA_{AP} were similar to those observed for $Co_{70}Fe_{30}$/MgO/$Co_{84}Fe_{16}$ MTJs (Ref. 53) and CMS/MgO/$Co_{50}Fe_{50}$ MTJs (Refs. 30 and 31). These results indicate that the decreasing TMR ratio with increasing T for the CCFA MTJs was mainly due to the RA_{AP} decrease. To clarify the reason for the strong T dependence of the TMR ratio, or equivalently that of the RA_{AP} observed for the CCFA/MgO/$Co_{50}Fe_{50}$ MTJs, further systematic study is needed.

IV. CONCLUSION

We fabricated fully epitaxial magnetic tunnel junctions (MTJs) with a full-Heusler alloy $Co_2Cr_{0.6}Fe_{0.4}Al$ (CCFA) thin film as a lower electrode, a MgO tunnel barrier, and a $Co_{50}Fe_{50}$ upper electrode. Pseudo-spin-valve-type, fully epitaxial CCFA/MgO/$Co_{50}Fe_{50}$ MTJs with a CCFA film composition close to the stoichiometric one demonstrated high tunnel magnetoresistance (TMR) ratios of 90% at room temperature (RT) and 240% at 4.2 K. These high TMR ratios were attributed to the increased spin polarization at the Fermi level, which was due to the increased ratio of the B_2 region to the A_2 region in CCFA films achieved by bringing the CCFA film composition close to the stoichiometric. Fully epitaxial CCFA/MgO/$Co_{50}Fe_{50}$ MTJs with exchange biasing were also fabricated, where a $Co_{50}Fe_{50}$ upper electrode was used in a synthetic ferrimagnetic $Co_{50}Fe_{50}$/Ru/$Co_{90}Fe_{10}$ trilayer exchange-iased with an IrMn layer through the $Co_{90}Fe_{10}$/IrMn interface. These exchange-biased CCFA/MgO/$Co_{50}Fe_{50}$ MTJs exhibited further enhanced TMR ratios of 109% at RT and 317% at 4.2 K. We suggested enhancement of the TMR ratio by a coherent tunneling contribution for fully epitaxial CCFA/MgO/$Co_{50}Fe_{50}$ MTJs.

These results confirm the promise of an epitaxial MTJ using a Co-based full-Heusler alloy as a key device structure for utilizing the potentially high spin polarization of this material system.

ACKNOWLEDGMENTS

The authors are grateful to Associate Professor Tetsuya Uemura, Associate Professor Masashi Arita, and Dr. Ken-ichi Matsuda for their helpful discussions and support. This work was partly supported by a Grant-in-Aid for Scientific Research (B) (Grant No. 18360143) and a Grant-in-Aid for Creative Scientific Research (Grant No. 14GS0301) from the Ministry of Education, Culture, Sports, Science and Technology, Japan. One of the authors (T.M.) was also supported by a Research Fellowship for Young Scientists from the Japan Society for the Promotion of Science.

[1] S. A. Wolf, D. D. Awschalom, R. A. Buhrman, J. M. Daughton, S. von Molnár, M. L. Roukes, A. Y. Chtchelkanova, and D. M. Treger, Science **294**, 1488 (2001).
[2] R. A. de Groot, F. M. Mueller, P. G. van Engen, and K. H. J. Buschow, Phys. Rev. Lett. **50**, 2024 (1983).
[3] T. Ambrose, J. J. Krebs, and G. A. Prinz, J. Appl. Phys. **87**, 5463 (2000).
[4] B. Ravel, J. O. Cross, M. P. Raphael, V. G. Harris, R. Ramesh, and V. Saraf, Appl. Phys. Lett. **81**, 2812 (2002).
[5] U. Geiersbach, A. Bergmann, and K. Westerholt, J. Magn. Magn. Mater. **240**, 546 (2002).
[6] S. Kämmerer, S. Heitmann, D. Meyners, D. Sudfeld, A. Thomas, A. Hütten, and G. Reiss, J. Appl. Phys. **93**, 7945 (2003).
[7] L. J. Singh, Z. H. Barber, Y. Miyoshi, Y. Bugoslavsky, W. R. Brandford, and L. F. Cohen, Appl. Phys. Lett. **84**, 2367 (2004).
[8] R. Kelekar and B. M. Clemens, J. Appl. Phys. **96**, 540 (2004).
[9] A. Hirohata, H. Kurebayashi, S. Okamura, M. Kikuchi, T. Masaki, T. Nozaki, N. Tezuka, and K. Inomata, J. Appl. Phys. **97**, 103714 (2005).
[10] K.-i. Matsuda, T. Kasahara, T. Marukame, T. Uemura, and M. Yamamoto, J. Cryst. Growth **286**, 389 (2006).
[11] T. Ishikawa, T. Marukame, K.-i. Matsuda, T. Uemura, M. Arita, and M. Yamamoto, J. Appl. Phys. **99**, 08J110 (2006).
[12] H. Kijima, T. Ishikawa, T. Marukame, H. Koyama, K. Matsuda, T. Uemura, and M. Yamamoto, IEEE Trans. Magn. **42**, 2688 (2006).
[13] S. Ishida, S. Fujii, S. Kashiwagi, and S. Asano, J. Phys. Soc. Jpn. **64**, 2152 (1995).
[14] S. Picozzi, A. Continenza, and A. J. Freeman, Phys. Rev. B **66**, 094421 (2002).
[15] P. J. Webster, J. Phys. Chem. Solids **32**, 1221 (1971).
[16] K. Inomata, S. Okamura, R. Goto, and N. Tezuka, Jpn. J. Appl. Phys., Part 2 **42**, L419 (2003).
[17] S. Kämmerer, A. Thomas, A. Hütten, and G. Reiss, Appl. Phys. Lett. **85**,

79 (2004).
[18]H. Kubota, J. Nakata, M. Oogane, Y. Ando, A. Sakuma, and T. Miyazaki, Jpn. J. Appl. Phys., Part 2 **43**, L984 (2004).
[19]Y. Sakuraba, J. Nakata, M. Oogane, H. Kubota, Y. Ando, A. Sakuma, and T. Miyazaki, Jpn. J. Appl. Phys., Part 2 **44**, L1100 (2005).
[20]S. Okamura, A. Miyazaki, S. Sugimoto, N. Tezuka, and K. Inomata, Appl. Phys. Lett. **86**, 232503 (2005).
[21]T. Marukame, T. Kasahara, K.-i. Matsuda, T. Uemura, and M. Yamamoto, Jpn. J. Appl. Phys., Part 2 **44**, L521 (2005).
[22]T. Marukame, T. Kasahara, K.-i. Matsuda, T. Uemura, and M. Yamamoto, IEEE Trans. Magn. **41**, 2603 (2005).
[23]Y. Sakuraba, J. Nakata, M. Oogane, Y. Ando, H. Kato, A. Sakuma, T. Miyazaki, and H. Kubota, Appl. Phys. Lett. **88**, 022503 (2006).
[24]Y. Sakuraba, M. Hattori, M. Oogane, Y. Ando, H. Kato, A. Sakuma, T. Miyazaki, and H. Kubota, Appl. Phys. Lett. **88**, 192508 (2006).
[25]K. Inomata, S. Okamura, A. Miyazaki, M. Kikuchi, N. Tezuka, M. Wojcik, and E. Jedryka, J. Phys. D **39**, 816 (2006).
[26]M. Yamamoto, T. Marukame, T. Ishikawa, K. Matsuda, T. Uemura, and M. Arita, J. Phys. D **39**, 824 (2006).
[27]T. Marukame, T. Ishikawa, K.-i. Matsuda, T. Uemura, and M. Yamamoto, J. Appl. Phys. **99**, 08A904 (2006).
[28]T. Marukame, T. Ishikawa, K.-i. Matsuda, T. Uemura, and M. Yamamoto, Appl. Phys. Lett. **88**, 262503 (2006).
[29]T. Marukame, T. Kasahara, K.-i. Matsuda, T. Uemura, and M. Yamamoto, IEEE Trans. Magn. **42**, 2652 (2006).
[30]T. Ishikawa, T. Marukame, H. Kijima, K.-i. Matsuda, T. Uemura, M. Arita, and M. Yamamoto, Appl. Phys. Lett. **89**, 192505 (2006).
[31]T. Marukame, H. Kijima, T. Ishikawa, K.-i. Matsuda, T. Uemura, and M. Yamamoto, J. Magn. Magn. Mater. **310**, 1946 (2007).
[32]H. Kijima, T. Ishikawa, T. Marukame, K.-i. Matsuda, T. Uemura, and M. Yamamoto, J. Magn. Magn. Mater. **310**, 2006 (2007).
[33]T. Marukame, T. Ishikawa, S. Hakamata, K.-i. Matsuda, T. Uemura, and M. Yamamoto, Appl. Phys. Lett. **90**, 012508 (2007).
[34]R. Kelekar and B. M. Clemens, Appl. Phys. Lett. **86**, 232501 (2005).
[35]K. Yakushiji, K. Saito, S. Mitani, K. Takanashi, Y. K. Takahashi, and K. Hono, Appl. Phys. Lett. **88**, 222504 (2006).
[36]X. Y. Dong *et al.*, Appl. Phys. Lett. **86**, 102107 (2005).
[37]M. C. Hickey *et al.*, Appl. Phys. Lett. **86**, 252106 (2005).
[38]Y. Miura, K. Nagao, and M. Shirai, Phys. Rev. B **69**, 144413 (2004).
[39]T. Block, C. Felser, G. Jakob, J. Ensling, B. Mühling, P. Gütlich, and R. J. Cava, J. Solid State Chem. **176**, 646 (2003).
[40]C. Felser *et al.*, J. Phys.: Condens. Matter **15**, 7019 (2003).
[41]K. Kobayashi, R. Y. Umetsu, R. Kainuma, K. Ishida, T. Oyamada, A. Fujita, and K. Fukamichi, Appl. Phys. Lett. **85**, 4684 (2004).
[42]S. Picozzi, A. Continenza, and A. J. Freeman, Phys. Rev. B **69**, 094423 (2004).
[43]S. S. P. Parkin *et al.*, J. Appl. Phys. **85**, 5828 (1999).
[44]W. C. Ellis and E. S. Greiner, Trans. Am. Soc. Met. **29**, 415 (1941).
[45]T. Ishikawa, T. Marukame, K.-i. Matsuda, T. Uemura, and M. Yamamoto, IEEE Trans. Magn. **42**, 3002 (2006).
[46]J. G. Simmons, J. Appl. Phys. **34**, 1793 (1963).
[47]S. Yuasa, T. Nagahama, A. Fukushima, Y. Suzuki, and K. Ando, Nat. Mater. **3**, 868 (2004).
[48]M. Jullière, Phys. Lett. **54**, 225 (1975).
[49]J. Mathon and A. Umerski, Phys. Rev. B **60**, 1117 (1999).
[50]D. J. Mosma and S. S. P. Parkin, Appl. Phys. Lett. **77**, 720 (2000).
[51]W. H. Butler, X.-G. Zhang, T. C. Schulthess, and J. M. Maclaren, Phys. Rev. B **63**, 054416 (2001).
[52]J. Mathon and A. Umerski, Phys. Rev. B **63**, 220403R (2001).
[53]S. S. P. Parkin, C. Kaiser, A. Panchula, P. M. Rice, B. Hughes, M. Samant, and S.-H. Yang, Nat. Mater. **3**, 862 (2004).